

The Geometry of the Vapor Layer Under a Leidenfrost Drop

J.C. Burton,* A.L. Sharpe, R.C.A. van der Veen, A. Franco, and S.R. Nagel
James Franck Institute and Department of Physics, The University of Chicago

(Dated: April 17, 2012)

In the Leidenfrost effect, liquid drops deposited on a hot surface levitate on a thin vapor cushion fed by evaporation of the liquid. This vapor layer forms a concave depression in the drop interface. Using laser-light interference coupled to high-speed imaging, we measured the radius, curvature, and height of the vapor pocket, as well as non-axisymmetric fluctuations of the interface for water drops at different temperatures. The geometry of the vapor pocket depends primarily on the drop size and not on the substrate temperature.

PACS numbers: 44.20.+b, 42.25.Hz, 47.55.nb

The nearly frictionless motion of water droplets on a hot pan is familiar to any cook. Such Leidenfrost drops [1] levitate on a thin, insulating cushion of evaporated vapor. Above a Leidenfrost temperature T_L there is a sudden increase in the drop lifetime [2, 3, 14] and the cessation of nucleated boiling. The stable vapor film, fed by the drop evaporation, drains under a thin annulus that resides closest to the substrate. Large Leidenfrost drops can undergo “star”-shaped oscillations [4–7], and a Leidenfrost vapor layer can reduce turbulent drag of a hot solid falling in a fluid [8]. In addition, individual Leidenfrost drops can propel themselves upon a ratcheted surface [9–11] as well as deposit micron-sized trails of nanoparticles [12]. Using light interference coupled to high-speed imaging, we measure the geometry of the vapor layer under a Leidenfrost drop. Although there are large fluctuations in its shape, over a wide range of temperatures a sustained vapor pocket exists whose average properties do not depend strongly on the evaporative flux from the drop.

We used reflected, monochromatic light to image thin vapor layers at high speeds, a technique we previously developed to study air layers beneath splashing droplets [13]. In the setup shown in Fig. 1(a), a fused-silica prism is encased in an aluminum block covering all its sides except the front face and a circular hole on the top. The temperature of the prism was regulated up to $T_s = 370^\circ\text{C}$. Above the Leidenfrost temperature $T_L \approx 160^\circ\text{C}$, drops of deionized water were deposited and were free to move in the circular hole. They were imaged until they completely evaporated, which occurred after a few minutes. The average temperature in the levitated drop was always $99 \pm 0.5^\circ\text{C}$ as measured with a thermistor. Near boiling, the density of water is $\rho = 958 \text{ kg m}^{-3}$ and the surface tension is $\gamma = 59 \text{ mN m}^{-1}$, so that the capillary length $\lambda_c = \sqrt{\gamma/\rho g} = 2.5 \text{ mm}$. For typical drop sizes used in our experiments, the gap height h_{neck} between the hot substrate and the bottom of the drop ranged from $5 \mu\text{m}$ to $100 \mu\text{m}$ (see Fig. 1(b), 2(a), and ref. [14]).

Although white-light interference has been used to measure vapor layers in drop impact when $h_{\text{neck}} \lesssim 5 \mu\text{m}$ [15], our experiments require illumination with a long

coherence length. The beam from a He-Ne laser with wavelength $\lambda_l = 632 \text{ nm}$ and coherence length $> 1 \text{ m}$ was expanded to a diameter of $\sim 3 \text{ cm}$ and sent into a prism at a small angle to prevent extraneous interference patterns generated between the faces of the prism and other optical elements. Only the gap between the substrate and the drop surface produced fringes. Approximately 3.5% of the light is reflected from the top surface of the prism and 2.1% from the bottom surface of the drop. The reflected light is imaged by a high-resolution camera (Prosilica GX3300) with an exposure time less than $100 \mu\text{s}$. High resolution was necessary to minimize Moiré effects where the fringe spacing is comparable to the pixel size. Simultaneously, we measure the drop radius, r_{max} , with white-light illumination from above and incident at a slight angle so that it reflects into the camera. Very recently we have been aware of a similar experimental setup used to study the collapse of the Leidenfrost vapor layer under an applied electric field [16].

The reflected light from the glass and liquid surfaces can interfere either constructively or destructively; the intensity is approximately $I \propto \sin(2\pi h/\lambda_l)^2$, where h is the distance between the substrate and the liquid surface. Thus the height difference between a black and a white fringe is $\lambda_l/4 = 158 \text{ nm}$. As shown in Fig. 1(c), fringes will be most visible in regions that are nearly flat (*i.e.*, $\nabla h \approx 0$). This occurs near the center of the gas pocket and in the thin annular neck surrounding it. This method can measure only variations in h but not its absolute value. Because the gas pocket acts as a weakly-focusing convex mirror, the center is surrounded by a bright region.

The fringes encode the geometry of the liquid surface. Fig. 1(c-d) shows fringe patterns around the neck of the drop, and the associated geometry of the liquid surface necessary to generate them. Saddle patterns are produced when the Gaussian curvature is negative, and circular patterns are produced when the Gaussian curvature is positive. Since the neck is closest to the surface, the curvature in the radial direction must be positive; thus the circular patterns around the neck represent local minima.

Fig. 2(a) shows the size of the neck at 4 different sur-

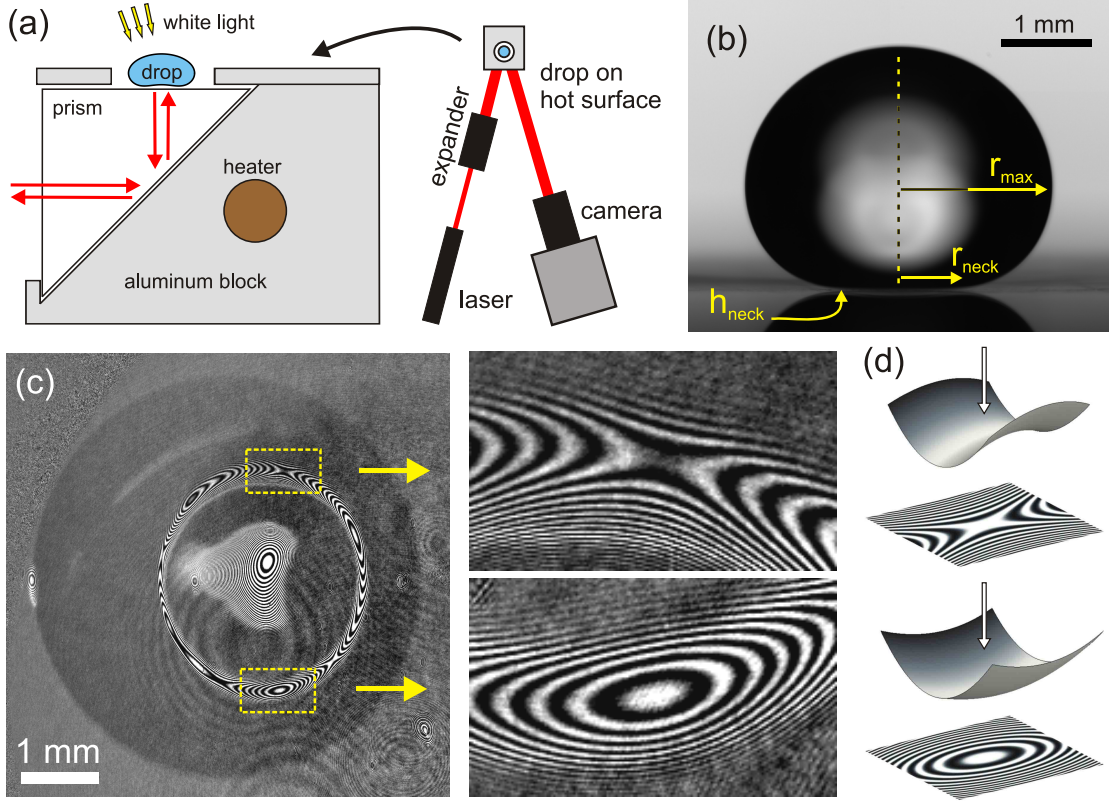


FIG. 1. (a) Schematic of measurement. Drops are deposited on a prism surface encased in a heated aluminum block. Reflected light from a He-Ne laser is imaged by a digital camera. Light interference occurs between the bottom surface of the drop and the top surface of the prism. White-light illumination enters the prism at a slight angle to produce a shadow that is slightly offset from the interference pattern. (b) Image of a water Leidenfrost drop from the side at substrate temperature $T_s = 320^\circ\text{C}$. The arrows indicate the maximum drop radius r_{max} , the radius of the neck r_{neck} , and the height of the neck from the surface h_{neck} . (c) Image from beneath a water Leidenfrost drop at $T_s = 245^\circ\text{C}$. The dark circular region is the shadow produced by the white light. Fringes are most visible in the neck region (outer ring interference pattern) and at the center of the gas pocket (inner concentric fringes). The zoomed-in images show saddle and circular patterns of fringes around the neck. (d) Saddle interference patterns are due to surfaces with negative Gaussian curvature; circular patterns are due to surfaces with positive Gaussian curvature.

face temperatures, T_s (and thus different evaporative gas fluxes). The neck radius, r_{neck} , is nearly independent of T_s and depends primarily on the drop radius r_{max} . There is significant scatter in the data for small drop sizes. At all temperatures, small drops sometimes bounce with an amplitude that is a significant fraction of the drop radius. We are unaware of any reported studies of this phenomenon. However, we speculate that the bouncing is due to coupling between the evaporation and capillary oscillations of the drop.

We estimate the shape of a stable, isothermal Leidenfrost drop in the limit of negligible internal flow following ref. [14, 17]. Most of the drop is surrounded by a constant atmospheric pressure. Therefore, r_{max} and r_{neck} depend on gravity and surface tension, identical to that of a drop on a superhydrophobic surface, where the liquid interface is tangent to the substrate at r_{neck} . Solving the Young-Laplace equation to obtain drop shapes [18], we

obtain for the superhydrophobic model the solid line in Fig. 2(b) which is in excellent agreement with the data.

For small drops, $r_{neck} \approx 0.8r_{max}^2/\lambda_c$, in agreement with [14, 17]. To calculate the prefactor, we note that inside a spherical drop the pressure is $P_{in} = 2\gamma/r_{max}$. As we will show, the vapor pocket becomes flat as $r_{max} \rightarrow 0$ so that the pressure under the drop is also P_{in} . This pressure must support the weight of the drop: $\frac{4}{3}\pi r_{max}^3 \rho g = \pi r_{neck}^2 P_{in}$. Thus for asymptotically small drops we have the exact result

$$r_{neck} = \sqrt{\frac{2}{3}} r_{max}^2 / \lambda_c \approx 0.82 r_{max}^2 / \lambda_c. \quad (1)$$

Large drops form flat “pancakes” with a thickness of order λ_c . There is a maximum size for a Leidenfrost drop before the gas pocket bubbles upward and turns the drop into a torus [14]. The maximum neck radius of a Leidenfrost drop was predicted to be $r_{neck} = r_{max} - 0.53\lambda_c$

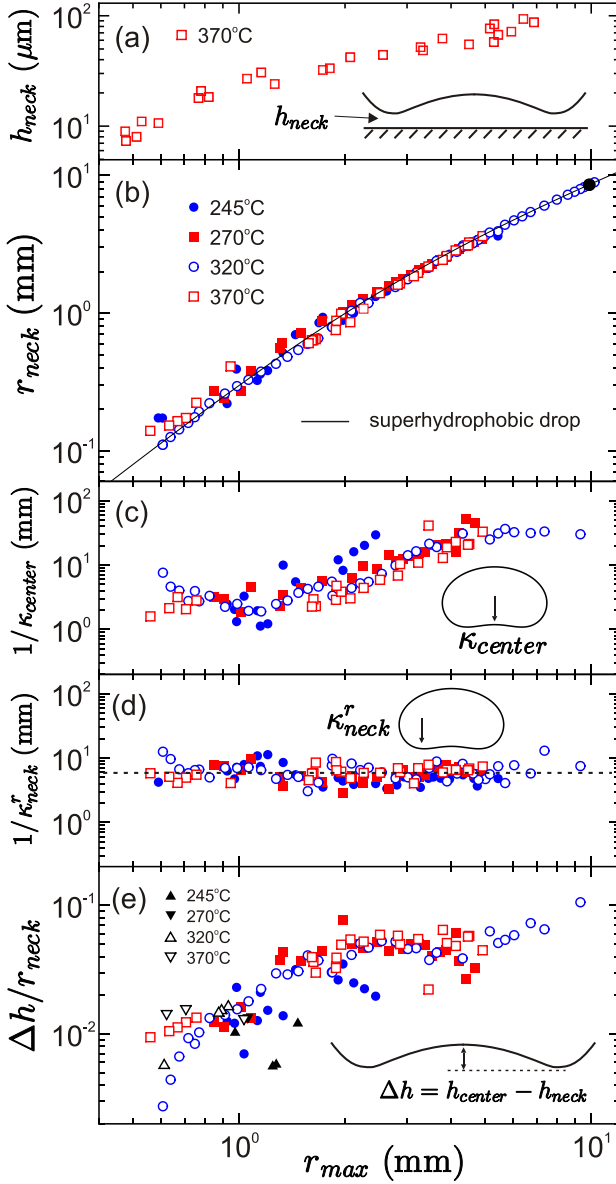


FIG. 2. Geometric measurements of the vapor interface versus r_{max} . (a) Height of the neck region from the surface measured from horizontal images such as Fig. 1(b). (b) Neck radius r_{neck} . The black line shows results from a model of a superhydrophobic drop. The solid black dot is the predicted maximum drop size [19]. (c) Average radius of curvature of the center $1/\kappa_{center}$ and (d) radial radius of curvature of the neck $1/\kappa_{neck}^r$ (indicated by the arrows). The horizontal dotted line in (d) represents $2.3\lambda_c$. (e) Aspect ratio of the vapor pocket. Black triangles are measured from drops with a continuous interference pattern from the neck to the center. Other symbols are from estimates using eqn. 2.

when $r_{max} \approx 3.95\lambda_c$, the maximum size of the drop at the initiation of the instability [19]. Our measurements of the maximum drop size and neck radius in Fig. 2(b) are within 4% of this prediction.

We also investigated the curvature of regions where fringes are visible. We measured the curvature at the center of the gas pocket, κ_{center} , averaged over two perpendicular directions given by the major and minor axes of the elliptical fringe pattern (Fig. 1(c)). We also studied the curvature of neck in the radial direction, κ_{neck}^r . Measurements of κ_{neck}^r are averaged over 4 points around the circumference of the neck. Fig. 2(c-d) shows that the radius of curvature is constant ($1/\kappa_{neck}^r \approx 2.3\lambda_c$), while $1/\kappa_{center}$ seems constant at both small and large drop sizes, but changes by a factor of ~ 10 between these regions. Both curvatures appear independent of T_s .

For small drops, we can observe the entire interference pattern from the neck to the center as shown in Fig. 3(a). We counted fringes to measure the difference in height, $\Delta h \equiv h_{center} - h_{neck}$. For larger drops we can estimate Δh by assuming a simple model for the geometry of the vapor pocket. Given two parabolas centered at $r = 0$ and $r = r_{neck}$ with respective curvatures $-\kappa_{center}$ and κ_{neck}^r , a unique value of Δh joins the two parabolas with a continuous derivative:

$$\Delta h = \frac{r_{neck}^2 \kappa_{center} \kappa_{neck}^r}{2(\kappa_{center} + \kappa_{neck}^r)}. \quad (2)$$

Fig. 2(e) shows the measured aspect ratio of the vapor pocket $\Delta h/r_{neck}$. The directly measured values agree well with the indirect measurements obtained with eqn. 2. Although the absolute height from the surface will certainly depend on the gas flux and thus the temperature of the surface, T_s , the data from Fig. 2 show that the geometry of the vapor pocket is nearly independent of T_s . The aspect ratio of the pocket $\Delta h/r_{neck}$ approaches zero for small drops, indicating an asymptotically flat geometry.

Fig. 3(a) shows an interference pattern for a small drop $r_{max} = 1.2$ mm, with a concave center region surrounded by the annular neck. For lower surface temperatures, large drops developed significant fluctuations in the geometry of the vapor pocket. Fig. 3(b) shows multiple extrema (concentric circular patterns), indicating a complex interfacial geometry. To quantify these fluctuations, we plot the number of extrema versus drop size for different temperatures in Fig. 3(c). Higher T_s and smaller drops produce only one extrema associated with the top of the vapor pocket, while lower T_s and larger drops tend to produce multiple extrema.

We next examine deviations from the axisymmetric description of a Leidenfrost drop. Fig. 1(c) and Fig. 3(a-b) show fringes around the circumference of the neck that allow us to calculate the height variation of the surface $\delta h_{neck}(\theta)$ versus azimuthal angle θ . Fig. 3(d) shows $\delta h_{neck}(\theta)/r_{max}$ for drops of different sizes. For small drops, there is a single wavelength variation around the neck. For larger drops, higher-order modes produce more complex profiles. Using data for the average value of h_{neck} from Fig. 2(a), we estimate that $\delta h_{neck}(\theta)$ can be as large as 20% of the average value of $h_{neck}(\theta)$.

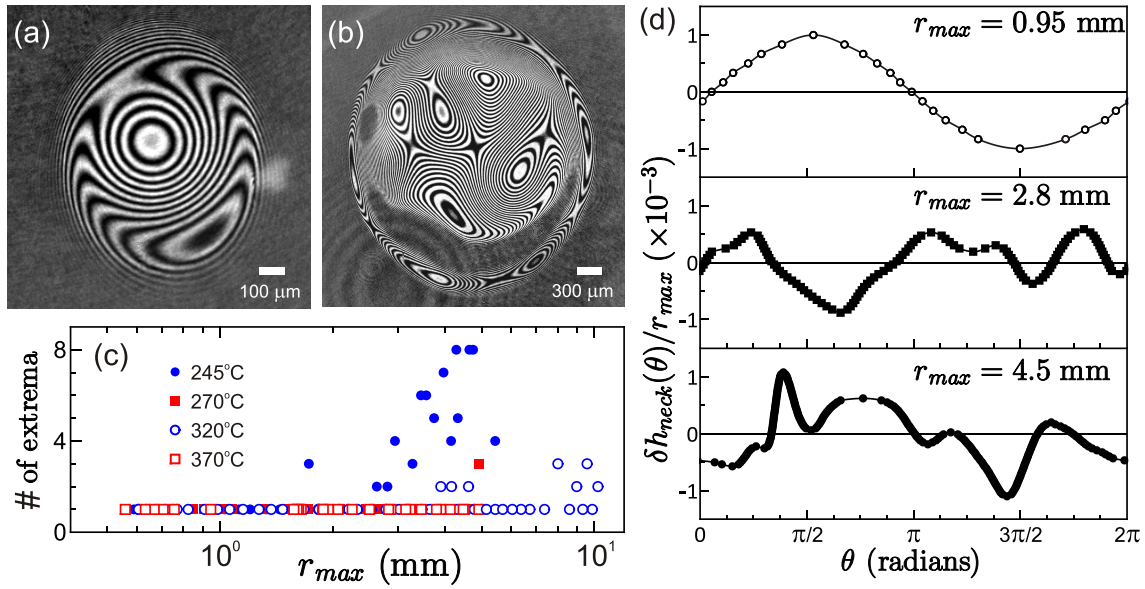


FIG. 3. Interference patterns at a surface temperature $T_s = 245^\circ\text{C}$, of (a) a small water drop $r_{max} = 1.2$ mm, and (b) a larger water drop $r_{max} = 2.7$ mm. The larger drops shows fluctuations in the inner gas pocket leading to a complex interference pattern. (c) Number of extrema (concentric circular patterns) in the inner gas pocket region. Small drops have a single maxima, while large drops at lower temperatures have multiple extrema due to a fluctuating liquid interface. (d) Variation of the neck height around its circumference for drops with $T_s = 370^\circ\text{C}$. Small drops with $r_{max} \ll \lambda_c$ have one wavelength of amplitude variation. Larger drops have higher modes of amplitude variation.

Counterintuitively, a drop on a very hot surface will survive for a surprisingly long time because it is levitated on an insulating layer of vapor. We have shown that the geometry of this insulating layer is nearly independent of substrate temperature, and depends only on the drop size. It becomes asymptotically flat for small drops. Moreover, significant fluctuations exist in the central vapor pocket and around the neck region by which the vapor escapes. These fluctuations vary quickly in time and space, and may be important for drop propulsion, oscillations and the “star”-shapes observed at high temperature.

We thank Michelle Driscoll, Taehun Lee and Jeff Morris for valuable discussions. We acknowledge support from NSF-PREM DMR-0934192 (JCB), NSF-MRSEC DMR-0820054 (RCAV), NSF DMR-1105145 (SRN), NSF REU PHY-1062785 (ALS), and NSF Materials World Network DMR-0807012 (AF) and use of the Keck Ultrafast Imaging Facility.

* jcburton@uchicago.edu

- [1] J. G. Leidenfrost, *De Aquae Communis Nonnullis Qualitatibus Tractatus* (Duisburg, 1756).
- [2] B. S. Gottfried and K. J. Bell, *Ind. Eng. Chem. Fund.* **5**, 561 (1966).
- [3] J. D. Bernardin, *J. Heat Transfer* **121** (1999).

- [4] P. Brunet and J. H. Snoeijer, *Eur. Phys. J. ST* **192**, 207 (2011).
- [5] N. Tokugawa and R. Takaki, *J. Phys. Soc. Jpn.* **63**, 1758 (1994).
- [6] K. Adachi and R. Takaki, *J. Phys. Soc. Jpn.* **53**, 4184 (1984).
- [7] D. Strier, A. Duarte, H. Ferrari, and G. Mindlin, *Physica A: Stat. Mech. App.* **283**, 261 (2000).
- [8] I. U. Vakarelski, J. O. Marston, D. Y. C. Chan, and S. T. Thoroddsen, *Phys. Rev. Lett.* **106**, 214501 (2011).
- [9] H. Linke, B. J. Alemán, L. D. Melling, M. J. Taormina, M. J. Francis, C. C. Dow-Hygelund, V. Narayanan, R. P. Taylor, and A. Stout, *Phys. Rev. Lett.* **96**, 154502 (2006).
- [10] G. Lagubeau, M. Le Merrer, C. Clanet, and D. Quéré, *Nat. Phys.* **7**, 395 (2011).
- [11] G. Dupeux, M. Le Merrer, C. Clanet, and D. Quéré, *Phys. Rev. Lett.* **107**, 114503 (2011).
- [12] M. Elbahri, D. Paretkar, K. Hirmas, S. Jebril, and R. Adelung, *Adv. Mater.* **19**, 1262 (2007).
- [13] M. M. Driscoll and S. R. Nagel, *Phys. Rev. Lett.* **107**, 154502 (2011).
- [14] A.-L. Biance, C. Clanet, and D. Quéré, *Phys. Fluids* **15**, 1632 (2003).
- [15] T. Tran, H. J. J. Staat, A. Prosperetti, C. Sun, and D. Lohse, *Phys. Rev. Lett.* **108**, 036101 (2012).
- [16] F. Celestini and G. Kirstetter, (2012), arXiv:1203.4799v1.
- [17] P. Aussillous and D. Quéré, *Nature* **411**, 924 (2001).
- [18] J. C. Burton, F. M. Huisman, P. Alison, D. Rogerson, and P. Taborek, *Langmuir* **26**, 15316 (2010).
- [19] J. H. Snoeijer, P. Brunet, and J. Eggers, *Phys. Rev. E* **79**, 036307 (2009).